Multichannel photoionization spectroscopy of Ar: Total cross section and threshold photoelectrons

Hugo W. van der Hart and Chris H. Greene
JILA and Department of Physics, Campus Box 440, University of Colorado, Boulder Colorado 80309-0440
(Received 6 April 1998)

Argon photoionization is studied using the *R*-matrix technique. Total photoionization cross sections, as well as partial cross sections for emission of a $3s$ electron, are obtained and compared with experimental results in the photon energy range between 30 and 38 eV. As a by-product of the photoionization calculations, threshold cross sections have been estimated for Ar^+ states up to 38 eV above the Ar ground state, and are compared with experiment. These comparisons show that the present approach can describe Ar autoionizing states reasonably well, even up to 38-eV photon energy. However, some modifications of previously used techniques have proven to be important in order to stabilize the calculation in this difficult energy range. [S1050-2947(98)05809-0]

PACS number(s): 32.80.Fb, 31.15.Ar, 31.50.+w

I. INTRODUCTION

Deviations of atomic dynamics from independent-particle behavior have challenged atomic physicists for the larger part of this century. One important process induced by the dielectronic repulsion is autoionization, in which an excited state decays nonradiatively. Independent-particle models describe this as a one-electron jump into a tighter-bound orbital, after which the excess energy donated to a second electron liberates it from the atom. Argon was one of the first atoms in which synchrotron radiation was used to probe autoionizing states [1]. Since this first observation over 35 years ago, many other studies have been devoted to Ar photoionization in the regime between 20 and 150 eV. Despite the rich multitude of resonances in this energy range that were observed and classified in Ref. [2], most subsequent experimental studies have focused on nonresonant photoionization features, such as the Cooper minimum at 48 eV [3–6].

At low photon energies, the photoionization of Ar is dominated by removal of a $3p$ electron. In the photon energy region between 26 and 29.24 eV, $3s3p^6np$ resonances appear, and the members up to $8p$ have recently been studied experimentally and analyzed using *R*-matrix calculations [7]. Above a photon energy of 29.24 eV, emission of a $3s$ electron becomes energetically allowed as well. Experiments [8–10] have determined accurate cross sections for this process, e.g., by measuring photoelectrons at the ''magic angle,'' although recently photon-induced fluorescence spectroscopy has been employed as well [11,12]. One feature of interest, theoretically predicted [13] and experimentally verified [8], is an apparent collective response of the electrons in the $n=3$ shell, which causes a Cooper minimum to appear at a similar energy in both $3s$ and $3p$ photoemission. This highly unusual coincidence might be taken as evidence that the underlying dynamics of these two subshells are coupled strongly. Recently, absolute experimental cross sections for photoionization of Ar with emission of a $3s$ electron have been reported, and the strong influence of autoionizing states of Ar in the photon energy range between 30 and 38 eV is immediately apparent [11]. These resonant states can dramatically affect the strength of interaction between the $3s$ and $3p$ subshells.

From a theoretical perspective, many approaches have been applied to Ar photoionization [14–18]. In most of these calculations, the determination of the atomic structure was restricted to the $3s3p^6np\ ^1P^o$ resonances. Above the $3s3p^6$ Ar^+ threshold, this restriction leads to a smooth spectrum. The collective response of the $n=3$ electrons leading to a minimum in the $3s$ photoemission at 43.8 eV prompted further calculations to study this emission process at higher frequencies [13,17,19–21].

The region containing argon doubly excited states has largely been avoided by theorists, because independent-particle techniques are better equipped to handle nonresonant processes. The first theoretical calculations examining the influence of doubly-excited states on photoionization processes in Ar were presented in Ref. [22]. Subsequently, Wijesundera and Kelly [23] employed many-body perturbation theory for another study. Reference [22] determined the total photoionization cross section and the partial photoexcitation cross sections of all $3p^44p$ states over the photon energy range from 36 and 52 eV, both theoretically and experimentally. It was found that electron interactions in the initial state are important to describe at a level more accurate than the independent-electron approximation, but that interactions in the final state are important for production of only a few final ionic states, such as $3p^4(^1D^e)4p\ ^2F^o$. Those earliest calculations were limited, however, since they included no Rydberg series or continua associated with the $3p^43d$ or $3p^44s$ thresholds. Wijesundera and Kelly [23] improved on the work of Ref. [22] by including Rydberg states attached to eight final Ar^+ states: the $3s^23p^5$, $3s3p^6$, $3p^4(^1D^e)nd\ ^2S^e$ with $3\leqslant n\leqslant 5$, and all $3p^44p\ ^2P^o$ states were included. The main focus of that study was aimed at a determination of photoexcitation (satellite) intensities for the $3p^4(^1D^e)nd\ ^2S^e$ states of Ar^+, which strongly interact with the $3s$ photoemission channel. While Ref. [23] reached a level of sophistication adequate to demonstrate the importance of doubly excited states in Ar $3p$ and $3s$ photoemission, it still could not show the full multichannel richness of the Ar photoionization spectra above 30 eV.

In this study, we present results for Ar photoionization in

the photon energy range between 30 and 38 eV, employing an extensive description of the Ar structure using the *R*-matrix approach. As such, the study is comparable to the theoretical calculations presented for Ne in Ref. [24]. The results discussed here include the total photoionization rates and partial cross sections for ejection of a 3*s* electron. Where possible we compare our theoretical description with experimental results, and assess the successes and failures of the present level of theory accordingly.

Another quantity of experimental relevance that is to some extent affected by doubly excited states is the threshold photoionization spectrum. The measurement of zero-energy electrons emitted from Ar after photoabsorption not only provides detailed information about the Ar^+ structure, but also about the spectrum of doubly excited states of Ar. In particular, the detachment of slow electrons is increased if a doubly excited state with a large transition probability from the ground state is found close to the threshold. Detailed experimental zero-energy electron spectra have been reported for Ar [25], and have been calculated as another byproduct of the present photoionization calculations. It should be noted that, by careful analysis of the threshold electron spectra, experimentalists have been able to retrieve the photoexcitation spectrum within 150 meV of the Ar^+ threshold [25,26].

II. THEORETICAL APPROACH

We adopt the multichannel quantum-defect *R*-matrix approach to describe the nonperturbative channel interactions, using techniques largely the same as those described in Ref. [27]. The approach employs a basis set expansion of the initial- and final-state wave functions within an inner region, while the final-state solutions in the outer region consist of Ar^+ eigenstates multiplied by Coulomb wave functions for the outermost electron, appropriately antisymmetrized. Solutions that remain continuous in value and derivative at the boundary are obtained by matching the inner and outer region solutions. The application of this version of *R*-matrix theory has been enhanced by combining it with another powerful approach in theoretical atomic physics, the multiconfiguration Hartree-Fock (MCHF) approach [28]. This combination has been successfully applied to the study of aluminum [29] and neon [24].

Accurate photoionization cross sections require an accurate description of both the initial and final states of the atom. The initial state is the Ar ground state. The final state can be viewed as a continuum photoelectron that moves in the field of many states of Ar^+ when it moves beyond the core, but within the *R*-matrix box it requires a more elaborate description as an eigenstate of the full Ar Hamiltonian. The presence of Ar doubly excited states in the energy range of interest in this paper implies that a good description of both Ar and Ar^+ is required simultaneously. The Ar final-state wave functions are approximated in the present calculation by adding a single electron to well-described low-lying states of Ar^+. These Ar^+ states are described using MCHF orbitals, which yield the best description that can be achieved with a small number of configurations.

The details of the MCHF expansion will be described in a forthcoming paper, so here we only give the essentials. The MCHF orbital set consists of physical $1s$, $\underline{2s}$, $\underline{2p}$, $3s$, $\underline{3p}$, $3d$, $4s$, and $4p$ orbitals together with $4d$, $5s$, and $5p$ pseudo-orbitals. The $1s$, $2s$, $2p$, $3s$, and $3p$ orbitals are optimized on the $1s^2 2s^2 2p^6 3s^2 3p^5$ state of Ar^+. The physical $n\ell = 3d$, $4s$ and $4p$ orbitals are then optimized on the average of the $1s^2 2s^2 2p^6 3s^2 3p^4 n\ell$ configuration using the previously determined inner orbitals. The pseudo-orbitals are generated by optimizing them on the three $3s^2 3p^4 n\ell$ states with the strongest configuration-interaction (CI) effects. A shorter CI expansion could be achieved through a separate optimization of different orbitals for every ionic eigenstate relevant to the energy range treated in the calculation, but the advantages in computational efficiency gained by using a common set of orthogonal orbitals far outweigh the separate optimization procedure.

After the MCHF orbitals have been generated, the basis set for Ar^+ in the photoionization calculations is constructed in the following way. For the $3s^2 3p^5$, $3s 3p^6$, and each $3s^2 3p^4 n\ell$ state with $n\ell$ a physical orbital, a configuration list including single and double excitations within the physical orbital set is generated. A CI calculation then gives the eigenvector of $3s^2 3p^5$, $3s 3p^6$, and $3s^2 3p^4 n\ell$ states. Every configuration with a coefficient of at least 0.03 in at least one expansion of an Ar^+ state is retained in the final Ar^+ basis. On average, these contributions total 99.4% of the Ar^+ state. The neglected contributions for one Ar^+ state may, however, be retained due to another Ar^+ state. Finally, pseudo-orbitals are added as $3s^2 3p^4 \overline{n\ell}$ configurations.

A CI calculation using this Ar^+ expansion gives the energies reported in Table I for states that can be excited by photoionization from the Ar ground state. The thresholds are labeled *a*–*t* for identification purposes. A comparison with the experimental energies [30] shows that the disagreement

TABLE I. Energies of Ar^+ states with respect to the $3s^2 3p^5\ ^2P^o$ state obtained in the *R*-matrix approach using MCHF orbitals and compared to the experimental results.

State	Label	*R* matrix (eV)	Expt. [30] (eV)
$3s^2 3p^5\ ^2P^o$	*a*	0.000	0.0
$3s 3p^6\ ^2S^e$	*b*	12.937	13.421
$3s^2 3p^4(^3P^e)4s\ ^2P^e$	*c*	17.452	17.123
$3s^2 3p^4(^3P^e)3d\ ^2P^e$	*d*	18.336	17.962
$3s^2 3p^4(^1D^e)4s\ ^2D^e$	*e*	18.696	18.384
$3s^2 3p^4(^3P^e)3d\ ^2F^e$	*f*	19.109	18.488
$3s^2 3p^4(^3P^e)3d\ ^2D^e$	*g*	19.124	18.643
$3s^2 3p^4(^1D^e)3d\ ^2G^e$	*h*	19.607	19.059
$3s^2 3p^4(^3P^e)4p\ ^2D^o$	*i*	20.098	19.654
$3s^2 3p^4(^3P^e)4p\ ^2P^o$	*k*	20.211	19.786
$3s^2 3p^4(^1D^e)3d\ ^2F^e$	*l*	20.924	20.201
$3s^2 3p^4(^1S^e)4s\ ^2S^e$	*m*	20.904	20.685
$3s^2 3p^4(^1D^e)4p\ ^2F^o$	*n*	21.532	21.077
$3s^2 3p^4(^1D^e)4p\ ^2P^o$	*o*	21.831	21.318
$3s^2 3p^4(^1D^e)3d\ ^2D^e$	*p*	22.205	21.329
$3s^2 3p^4(^1D^e)4p\ ^2D^o$	*q*	22.002	21.437
$3s^2 3p^4(^1D^e)3d\ ^2P^e$	*r*	23.079	21.582
$3s^2 3p^4(^1S^e)3d\ ^2D^e$	*s*	22.993	22.224
$3s^2 3p^4(^1D^e)3d\ ^2S^e$	*t*	23.573	22.766

in excitation energy is generally around 0.5 eV, but that for the highest $3s^2 3p^4(3d,4s,4p)$ states the average discrepancy increases up to 1.5 eV. These highest states lie close to the energy region where higher-lying $3p^4 n\ell$ states are found, which have been omitted from the present calculation to keep its size manageable. The neglect of these terms results in a deterioration of the quality of our description for the high-lying Ar^+ states. In fact, the $3s^2 3p^4(^1S^e)4p\ ^2P^o$ state is immersed in these higher manifolds, and no reliable theoretical prediction can be provided. Moreover, the excitation energy of the lowest excited states is too low, a further indication that the Ar^+ ground-state wave function is not fully converged.

Except for some exploratory calculations performed to assess convergence with respect to box size, the present calculations utilized a box radius of 13 a.u. The Ar basis set consists of the Ar^+ states combined with a set of ''outermost electron states'' having $\ell \leqslant 3$. This set contains 21 states for *s* and *p* electrons, 18 for *d* electrons, and 16 for *f* electrons. The total basis expansion for the Ar photoionization problem then consists of 2350 states for the $^1S^e$ states and 5581 for the $^1P^o$ states. The ground-state energy of Ar is calculated to be -17.755 eV, compared to the experimental results of -15.819 eV, relative to the ground state of Ar^+. The ground-state binding energy is overestimated, because we have used a much larger CI expansion for the Ar ground state than for the Ar^+ states. In order to obtain the proper transition frequencies at the thresholds, the Ar ground state and all Ar^+ states are shifted to the experimental values.

This overconvergence can be explained through core-polarization interactions. Suppose that the binding energy of interest is the ground-state binding energy, the energy difference between the $3s^2 3p^6\ ^1S^e$ and $3s^2 3p^5\ ^2P^o$ states. The excitation of two electrons from the $3p$ to $3d$ shell gives a configuration interacting with both the Ar and the Ar^+ ground states. For Ar this configuration is $3s^2 3p^4 3d^2$, whereas, for Ar^+, this gives $3s^2 3p^3 3d^2$. In determining the photoexcitation of Ar doubly excited states, the Ar configuration is included automatically through an important excited Ar^+ target configuration, $3s^2 3p^4 3d$, whereas special efforts are required to include the $3s^2 3p^3 3d^2$ configuration for Ar^+. Moreover, for consistency the inclusion of this target state also enlarges the basis set for Ar with configurations, such as $3s^2 3p^3 3d^2 n\ell$. When all possible excitations are included, the correct energy difference will be reproduced, but in other cases the Ar binding energy is easily overestimated. Since the Ar^+ and Ar basis sizes are inextricably linked to each other, the only way to improve on this overconvergence is by extending both basis sets.

The shifts of the Ar^+ states have been included in a different manner from the one detailed in Ref. [27]. Due to the number of target states and open channels, and the relatively large shifts of the Ar^+ states, shifting the Ar^+ energies in the quantum-defect part of the approach does not produce stable results. The approach has thus been modified. Before the evaluation of the *K* matrices, the shifts of the Ar^+ states are determined from the eigenvalues of the Ar^+ Hamiltonian. These shifts are then transformed back to shifts for the Ar^+ basis states, including off-diagonal interactions. Since the Ar states are described as an Ar^+ basis state plus a continuum electron, these shifts and off-diagonal interactions can be directly added to the Ar Hamiltonian. This modified Hamiltonian is then employed to determine the Ar photoionization properties. This approach leads to significantly more stable values for all channels. The energies of configurations like $3s^2 3p^3 3d^3$ have not been shifted, but the influence of these configurations is comparatively small.

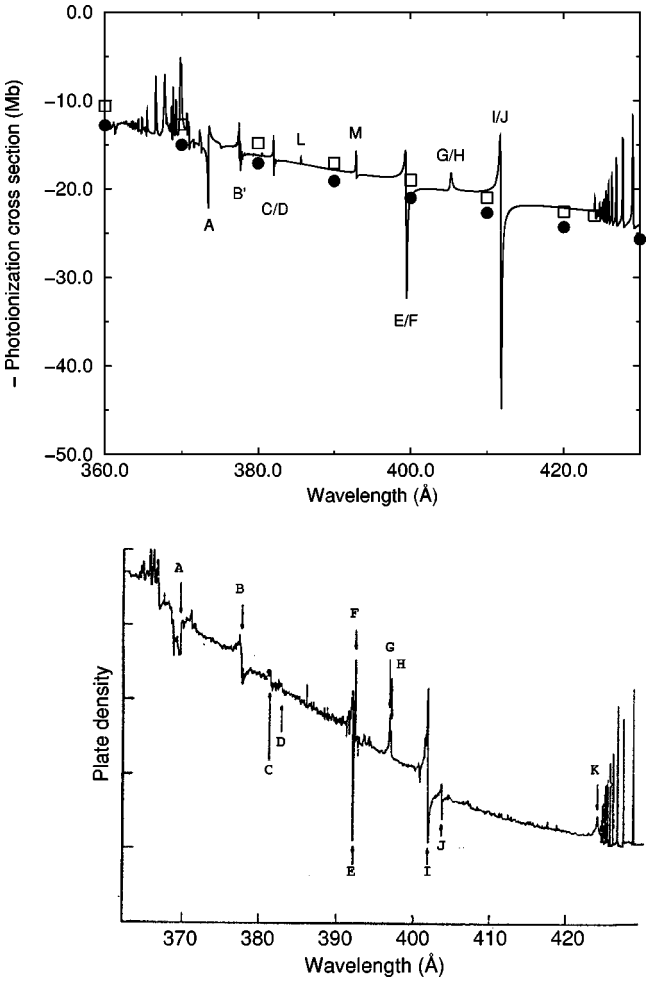

FIG. 1. Total photoionization cross sections for Ar above the threshold for ejection of a $3s$ electron. In the top figure, the *R*-matrix results are indicated by a solid line, and compared to the results of Samson *et al.* [31] (open squares) and the compilation of Marr and West [5] (full circles). The bottom figure shows Fig. 3 from the report by Madden, Ederer, and Codling [2].

III. RESULTS AND DISCUSSION

A. Total photoionization

The total photoionization cross section of Ar in the energy range above the threshold for detachment of a $3s$ electron is shown in Fig. 1. The theoretical spectrum is compared with the measurements of Ref. [31] and the compilation of Marr and West [5]. To test our theoretical description of the resonance structures, the results are also compared with the early but detailed photographic measurements carried out in Ref. [2] in the wavelength region between 360 and 430 Å. Since the experimental results have been obtained as a function of wavelength, we also present our spectrum in Å units. The identification in [2] of the resonances marked *A*–*K* is given

TABLE II. Identification and energy of the resonances *A*–*M* as indicated in Fig. 1. Resonance B' is our identification of resonance *B*. The wavelengths are averaged over j of the outer electron.

Resonance	Identification [2]	Wavelength [2] (Å)
A	$3p^4(^1S^e)4s(^2S^e_{1/2})4p$	369.93±0.02
B	$3p^4(^1D^e)3d(^2F^e_{5/2})4p$	377.40±0.02
B'	$3p^4(^1D^e)4s(^2D^e)5p$[a]	
C	$3p^4(^3P^e)3d(^2P^e_{3/2})5p$	381.14±0.04
D	$3p^4(^3P^e)3d(^2P^e_{1/2})5p$	382.82±0.03
E	$3p^4(^3P^e)3d(^2D^e_{3/2})4p$	391.29±0.03
F	$3p^4(^3P^e)4s(^2P^e_{1/2})5p$	392.22±0.04
G	$3p^4(^1D^e)4s(^2D^e_{5/2})4p$	396.76±0.02
H	$3p^4(^1D^e)4s(^2D^e_{3/2})4p$	396.99±0.02
I	$3p^4(^3P^e)3d(^2P^e_{3/2})4p$	401.15±0.03
J	$3p^4(^3P^e)3d(^2P^e_{1/2})4p$	403.76±0.03
K	$3p^4(^3P^e)4s(^2P^e_{1/2})4p$	424.23±0.02
L	$3p^4(^3P^e)4s(^2P^e)7p$[a]	
M	$3p^4(^3P^e)4s(^2P^e)6p$[a]	386.21±0.04

[a]Present work.

in Table II, and by indicating these resonances also in the theoretical spectrum, the analogies and differences can be estimated for these resonances. Uppercase letters are used to indicate Ar states, while lowercase is reserved for Ar^+ thresholds. The experimental results have been obtained with a resolution of 0.06 Å or roughly 5 meV at the photon energies of interest. The theoretical results were accordingly convolved with a Gaussian of 5 meV (full width at half maximum) to simulate this resolution. Over the entire wavelength range below 430 Å, neutral Ar resonances are observed. Although many other experiments have been performed [3–6], the spectra of Ref. [2] still characterize the resonance features in the wavelength range from 360 to 430 Å with the greatest accuracy to date.

We classify resonance *B* differently than Ref. [2], since the $3p^4(^3P^e)3d(^2F^e)4p\ ^1P^o$ state is not allowed in *LS* coupling, which possibly suggests a typographical error in their paper. Our calculations indicate that $3p^4(^1D^e)4s(^2D^e)5p\ ^1P^o$ is a more appropriate characterization. In fact, Madden and Codling associated a resonance close to the $3p^4(^3P^e)3d(^2F^e)4p\ ^1P^o$ state with the $3p^4(^1D^e)4s(^2D^e)5p\ ^1P^o$ resonance. It should be noted that for several of the resonances, e.g., resonances *E*,*F* and *G*,*H*, it is quite difficult to obtain an unambiguous classification due to the large interactions between the Ar resonances. Two additional resonances are seen in between wavelengths of 380 and 390 Å, and their identification is also given in Table II. Resonance *M* has been identified as such by Ref. [2], and their experimental transition wavelength is also reported.

Although the present calculation is limited to *LS* coupling, with all fine-structure effects neglected, generally good agreement is found with experiment. The total photoionization cross section is typically within about 1.5 Mb of the experimental results. Our calculations achieve a poorer description of the energy-dependent decrease of the photoionization cross section with decreasing wavelength; this reflects our position of the Cooper minimum at 49.7±1.0 eV, with the uncertainty in the position arising from resonances in the photoionization spectrum, as will be discussed in more detail for the $3s$ photoemission. These differences can be ascribed predominantly to limitations in our description of both the Ar and Ar^+ ground states. The emphasis is on the description of the structure up to a photon energy of 38 eV, which means that we require a good description of 26 channels simultaneously. The most difficult channels to describe are of $3p^4n\ell$ character, and hence no special effort has been made to obtain the best agreement for the background rate and the position of the Cooper minimum for the $3p$ photoemission channel. Nevertheless, the background behavior of the total photoionization is described quite well.

By comparing the present results with the experimental ones [2], it can be seen that the overall agreement is quite good. There are definite differences in the position of certain resonances, but the shape of the spectra is in reasonable agreement. One example of a resonance feature not resolved experimentally is apparent for resonance *B*, which shows up as a single experimental resonance, while the calculations also show an interference with the Rydberg series converging to the $3s^23p^4(^3P^e)4s\ ^2P^e$ threshold at a slightly shorter wavelength. Below a wavelength of 370 Å the number of resonances increases considerably, but here a good description of the photoionization spectrum is also obtained. The relative intensities of the resonances are, however, not described very well, as can be seen in the neighborhood of resonance *A*.

The calculated energies of certain resonances are not very accurate. For instance, the wavelength for the transition from the ground state to the average $3p^4(^3P^e)4s(^2P^e)4p\ ^1P^o$ state, resonance *G*,*H*, differs from experiment by roughly 8 Å or 2%. In energy, this corresponds to a disagreement of 0.7 eV, and a difference in quantum-defect of $\Delta n^* = 0.23$. We typically strive for quantum-defect errors less than about 0.05, so the present discrepancy is regarded as signifying some qualitative problems with our multichannel wave functions. The origin of this deviation is essentially the same as the one causing the overbinding of the Ar ground state: the expansion for the Ar states contains more configurations, and is able to describe a fuller range of core-polarization effects than the Ar^+ basis set. Consequently, those Ar states that are most affected by core polarization converge to energies that are too far below their respective thresholds. This problem therefore stands out particularly for low-lying states in the Rydberg series, but for states higher up in the series, this problem should be less serious, since the polarization potential drops off with r^{-4}.

Another discrepancy can be noticed in the long-wavelength part of the spectrum, where the experimental $3p^4(^3P^e)3d(^2P^e)4p\ ^1P^o$ resonance is split into two separate peaks, resonances *I* and *J*, by spin-orbit coupling. The calculations, of course, are carried out in an *LS*-coupling approximation, with all fine-structure terms omitted from the Hamiltonian. This means that the different J levels of the $3p^4(^3P^e)3d\ ^2P^e$ threshold are degenerate. Consequently, adding a Rydberg electron to this state to form a $^1P^o$ state results in two degenerate states instead of fine-structure-split peaks. Similarly, only one $3p^4(^3P^e)4s(^2P^e)4p\ ^1P^o$ state is calculated, lying below the $3s3p^6\ ^2S^e$ state, while experimentally two are observed, one above (resonance *K*) and one below the $3s3p^6\ ^2S^e$ threshold due to the lifting of the J

degeneracy. Such discrepancies between theory and experiment are observed throughout the spectrum, whenever the spin-orbit splitting of the threshold is large.

Despite these differences between theory and experiment, the agreement in the shape and structure of the experimental and theoretical spectra shows that employing the combination of *R*-matrix and MCHF techniques a reasonable overall interpretation of the spectrum can be obtained. It provides a reliable identification of most observed resonances, and allows us to assess the nature of the dominant channel interactions in this energy range of Ar photoionization.

B. Emission of a 3*s* electron

Above a photon energy of 29.24 eV, it is energetically allowed to excite the residual Ar^+ ion simultaneously with the emission of an electron. The lowest excited state is the $3s3p^6\ ^2S^e$ state and its excitation therefore corresponds to emission of a 3*s* electron. Several approaches have been applied to study this process experimentally in the energy range between 30 and 38 eV [8–10]. A resolution of 90 meV, was achieved by Möbus *et al* [11], but recently they significantly improved their resolution [12]. This latter study indicates that the observed structure in the experimental data corresponds to atomic structure, and is not due to experimental uncertainties.

Möbus *et al.* compared their results with theoretical data [13,17,19–21,23], but while these calculations provide a good description of the nonresonant photoionization behavior, no agreement was obtained for the resonant photoionization spectrum. To a limited extent, Wijesundera and Kelly [23] included channel interactions in the final-state expansion that they adopted to describe the Ar ionization continuum. In addition to the $3s^23p^5$ and $3s3p^6$ Ar^+ states, they included the $3s^23p^4(^1D^e)md(^2S^e)$ Ar^+ thresholds (with $3 \leqslant m \leqslant 5$), owing to their strong interaction with the $3s3p^6$ channel, and the three $3s^23p^44p\ ^2P^o$ states of Ar^+. While their description does produce Ar resonances in the frequency range of interest, the resonant portion of the calculated spectrum does not agree with experiment [11]. Notably, the experiment shows a significant amount of structure from 32 to 35 eV which is absent from the calculations. On the other hand, at frequencies larger than 40 eV, where the resonant Ar spectrum is less important than the e^--Ar^+ open-channel interactions, the cross sections obtained by Wijesundera and Kelly [23] for excitations of the $3s^23p^4n\ell$ states are in excellent agreement with the experimental results [32].

The cross section obtained from our *R*-matrix calculation in Fig. 2 is seen to overestimate the experimental results obtained by Möbus *et al.* [11], by roughly 0.2 Mb. Such a difference is not too surprising, since we have optimized the basis set to describe many high-lying states as accurately as possible. Our primary goal in this paper is to achieve a reasonable description of the resonance structures. Although the resonance positions differ from experiment by about 0.7 eV ($\Delta n^* = 0.23$) in the region between 30 and 32 eV, Fig. 2 shows that we have achieved reasonable success in reproducing much of the fine detail observed experimentally. Just below 34 eV a large decrease in the photoionization is observed both in theory and experimentally. Both theory and experiment give a two-step increase in photodetachment at frequencies just above 34 eV. Not only is the global structure of the spectrum reproduced, but the numerous smaller structures in the spectrum are also accounted for.

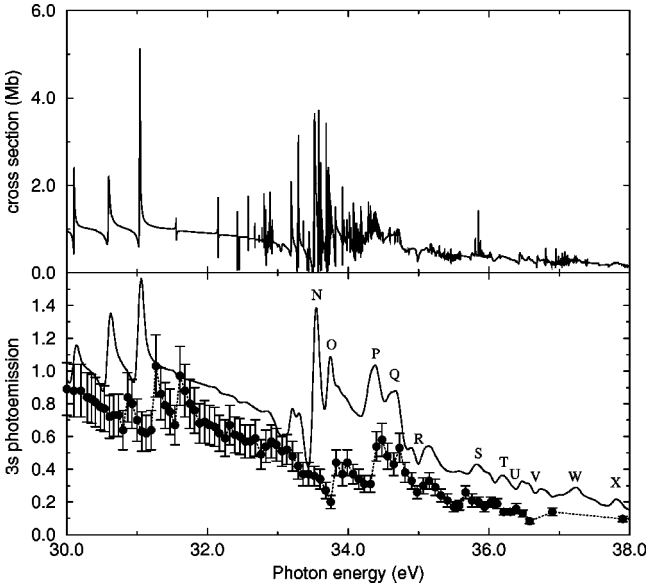

FIG. 2. Photoionization cross sections of Ar with emission of a 3*s* electron determined using the *R*-matrix approach (solid line). In the top figure, the final spectrum is given without applying any convolution, while in the bottom figure the spectrum is convolved with the experimental resolution of 90 meV. The experimental results [11] are also indicated in the bottom figure by filled circles connected by a dotted line.

As mentioned in Sec. I, the 3*s* photoemission shows a Cooper minimum at a roughly similar photon energy as observed in the 3*p* photoemission [13,8]. The experimental position of the Cooper minimum, which lies outside the photon energy region shown in Fig. 2, compares at 43.8 eV reasonably well with the position obtained employing the present Ar and Ar^+ expansions, 44.1 ± 1.0 eV. The uncertainty in the position is caused by the presence of resonances arising from Rydberg series converging to high-lying states of Ar^+ such as those belonging to the $3s3p^43d^2$ configuration. Moreover, unphysical resonances may appear in this region, since the Ar photoionization channels opening beyond the $3s^23p^4(^1D^e)3d\ ^2S^e$ threshold of Ar^+, labeled *t* in Table I, remain artificially closed in order to keep the calculations feasible. Additionally, the limitations in the present Ar description further limit the accuracy with which the position of the Cooper minimum can be determined.

The agreement between theoretical and experimental resonance properties is close enough to permit us to classify the observed resonances by examining their channel composition. Several Ar resonances have been identified in the convolved theoretical spectrum (resonances *P*–*X*), and these are classified in Table III. Although many resonances are present in this photon energy region, due to the finite experimental resolution only a comparative few are observed experimentally. It should be mentioned that for a proper identification of the resonances observed in experiment, a knowledge of the experimental resolution is essential. The energy difference between subsequent members of the Rydberg series is given in a.u. by $Z_c^2/(n-\delta)^3$, with δ the quantum defect and

TABLE III. Identification of resonances observed in the theoretical photoionization spectrum. The labels correspond to those in Fig. 2. The energies correspond to the observed position in the theoretical spectrum. These energies may differ from the experimental positions. The identification consists of the threshold associated with the resonance, the effective quantum number and the state of the outer electron. Window resonances are indicated by w and peaks are indicated by *p*.

Label	Energy (eV)	Ar^+ threshold	n^*	Outer electron	Type
N	33.55	$3s^2 3p^4(^1D^e)4s\ ^2D^e$	4.56	*6p*	*p*
O	33.75	$3s^2 3p^4(^1D^e)4s\ ^2D^e$	5.47	*7p*	*p*
P	34.38	$3s^2 3p^4(^3P^e)4p\ ^2P^o$	3.33	*4d*	*p*
Q	34.67	$3s^2 3p^4(^3P^e)4p\ ^2P^o$	3.75	*6s*	*p*
R	35.00	$3s^2 3p^4(^3P^e)4p\ ^2P^o$	4.73	*7s*	*w*
S	35.83	$3s^2 3p^4(^1D^e)4p\ ^2F^o$	3.57	*4d*	*p*
T	36.19	$3s^2 3p^4(^1D^e)4p\ ^2F^o$	4.39	*5d*	*p*
U	36.38	$3s^2 3p^4(^1D^e)3d\ ^2D^e$	4.21	*6p*	*w*
V	36.66	$3s^2 3p^4(^1D^e)3d\ ^2D^e$	5.28	*7p*	*w*
W	37.23	$3s^2 3p^4(^1D^e)3d\ ^2S^e$	3.17	*5p*	*p*
X	37.81	$3s^2 3p^4(^1D^e)3d\ ^2S^e$	4.19	*6p*	*p*

Z_c the net charge seen by the Rydberg electron. In order to resolve subsequent members of the Rydberg series as individual peaks, the experimental resolution must be smaller than this energy difference. Since this energy difference decreases with n, higher n states cannot be isolated, and in fact a maximum n value can be determined beyond which states can no longer be separated. States with lower n values can be much broader than the experimental resolution, and the excitation peak for such a resonance may be split into several peaks due to interferences with another Rydberg series. An example of this is the $3p^4(^1D^e)3d(^2F_{5/2})4p\ ^1P^o$ state (resonance B') in Fig. 1 for which the states in the overlapping Rydberg series can be identified in the theoretical cross sections. Thus, while the unconvolved spectrum in Fig. 2 shows a multitude of resonances in the photon energy range between 33 and 35 eV, the much smoother experimental spectrum is reproduced only after a convolution with the experimental resolution. Consequently, it is very difficult to identify the experimentally observed resonances from the comparison with the unconvolved spectrum.

At the low-energy side in Fig. 2, three strong resonances are visible, which can be identified from the total photoionization spectra in Fig. 1 as $3p^4(^3P)3d(^2P)4p\ ^1P^o$ and $3p^4(^1D)4s(^2D)4p\ ^1P^o$, and an overlap of $3p^4(^3P)4s(^2D)5p\ ^1P^o$ and $3p^4(^3P)3d(^2D)4p\ ^1P^o$ from low to high energy. Above an energy of 33 eV, several resonances appear in the experimental spectrum in Fig. 2. Many of these resonances consist of overlapping states, but Table III presents our classification of 11 resonances in the convolved theoretical spectrum. The table indicates which Rydberg series have the strongest influence on the 3s photoemission, but the subtler effects of the channel interactions can only be observed after a careful analysis of the resonance line shapes. For instance, resonances *P* and *Q*, at 34.69 and 35.00 eV, respectively, are identified as the *6s* and *7s* states in the Rydberg series converging to the $3p^4(^3P^e)4p\ ^2P^o$ state. The *6s* state is a peak resonance, while the *7s* state appears as a window resonance. This qualitative change in line shapes from one state in a Rydberg series to the next is caused by interactions with other (broad) perturbing resonances.

Although most of the resonances observed in the experimental spectrum lie reasonably close to the position derived from our theoretical calculation, this is not the case for resonances *N* and *O* at 33.55 and 33.75 eV, respectively, whose experimental analogs appear in between 33.8 and 34.0 eV. (Experimental spectra obtained with an improved resolution indicate that these indeed belong to two different resonance structures [12].) This difference between theory and experiment indicates that an underlying resonance is responsible for the large increase in the photoionization at 33.6 eV. By examination of the theoretical spectra, this resonance is found to be the $3p^4(^3P^e)4p(^2P^o)5s\ ^1P^o$ state. The higher members of this series are observed as individual resonances *P* and *Q* (see also Table III) in the photoionization spectrum, and quantum-defect extrapolation from these two states predicts a position for the $5s$ resonance around 33.8 eV. The $3p^4(^3P^e)4p(^2P^o)5s\ ^1P^o$ state strongly interacts with the $3s^2 3p^4(^1D^e)4s(^2D^e)np\ ^1P^o$ Rydberg series, and the Rydberg states consequently obtain a significant amount of the final population and appear as prominent resonances in the spectrum. From a comparison with the experimental spectra, it appears that this underlying resonance is shifted to lower energy by about 0.2 eV.

This discussion shows that the incorrect positions of the resonances affect the interference effects. These incorrect positions are ascribed mainly to inaccuracies in the truncated CI expansion of the Ar^+ states. Thus the interaction strength between Rydberg series, which is assumed to be a fairly smooth function of energy, is described to a better degree. However, a different position of the resonances may also affect the interference by changing constructive interference into a destructive one, or vice versa. As shown in Fig. 2, there are still large differences between the experimental and theoretical excitation cross sections, especially in the photon energy region from 33 to 35 eV, which indicate that there are some qualitative features in the calculated wave functions, that are in error and should be improved upon in subsequent work.

C. Threshold photoelectron spectra

Another property of recent experimental interest is the threshold photoionization spectrum of Ar. For example, in the measurements in Ref. [25], the probability of leaving Ar^+ in an excited state with the outgoing electron having an energy in the range 0 up to roughly 25 meV is measured. Threshold spectra have now been measured with fine accuracy from the onset of the doubly excited states up to the $3p^4\ ^1S^e$ threshold of Ar^{2+} [25,33–35]. These experiments not only probe the structure of Ar^+, since electrons can only be emitted within a finite energy of an Ar^+ state, but also the structure of Ar, since the threshold photoionization can be enhanced considerably by doubly excited states straddling the threshold. Thus theoretical predictions for the threshold intensities need to take the structure of Ar into account.

Several theoretical calculations have been performed to estimate the threshold intensities [22,35]. Most of the calcu-

lations apply the sudden approximation, in which the excited electron is assumed not to interact with the remaining electrons after absorption of a photon. The threshold intensities in this approach are (to this level of approximation) governed directly by configuration interaction in the initial and final states. As we discussed above, the photoionization cross section exhibits a great deal of structure in the range between 30 and 38 eV. Experimentally, large influences from Ar** resonances have already been observed for photoionization with excitation of the $3p^4n\ell$ states [36], especially within 4 eV of the threshold. The validity of the sudden approximation is therefore questionable at energies within 4 eV of the thresholds of interest. The present calculation includes the doubly excited states, and is therefore able to determine threshold photoionization cross sections including contributions from Ar autoionizing states.

The probability for emitting an electron with energy less than 25 meV can be calculated from the partial photoionization cross sections for excitation of the $3p^4n\ell$ states, which will be detailed in a separate paper. The experimental photon energy resolution is 25 meV, so we first convolve the theoretical photoexcitation spectra with a Gaussian of width 25 meV. The zero-electron-energy spectrum for each partial channel is then calculated by multiplying the convolved spectra by a photoelectron energy-dependent weight factor, which falls rapidly to zero for emitted electron energies larger than 25 meV. The actual form chosen is

$$W=\frac{1}{\exp(E-E_T-E_c)/E_w+1}, \tag{1}$$

with E_T the threshold energy, E_c the cutoff energy, and E_w a constant, which is set to 2.5 meV in the present case. Due to the convolution, the channel is already opened slightly before the threshold energy is reached, which simulates the probable Stark field ionization of very high Rydberg levels lying just below each ionic threshold. Finally, all partial spectra are summed to yield the total threshold ionization spectrum.

The results are presented in Fig. 3, together with experimental results [25]. The latter are relative measurements, so we have normalized the maximum experimental intensity of the $3p^4(^1D^e)4s\ ^2D^e$ state (threshold *e*) to coincide with our calculated result. An accurate quantitative comparison is hindered by the fact that our calculations have been performed in *LS* coupling. The spin-orbit splitting of the true Ar^+ states causes overlaps between different ionization thresholds and splits the contribution from one *LS* peak into two or more peaks. Yet another complication is the fact that quartet states can also be populated through spin-orbit interactions that have been entirely neglected in the present calculations.

In the energy region between 32 and 36 eV, a fairly good description of the experimental spectrum is obtained. The excitation intensity of the $3s^23p^4(^3P^e)3d\ ^2P^e$ state (threshold *d*) is found to be the strongest, and this intensity is second strongest for the $3s^23p^4(^3P^e)4s\ ^2D^e$ state (threshold *e*). Due to the splitting of the $^2P^e$ peak, it is difficult to estimate the relative intensities of the two, but the theoretical result appears to agree with experiment. The excitation of threshold *c* in Fig. 3 is in some disagreement. This difference can be explained from Fig. 1, in which resonance B' is perturbed by

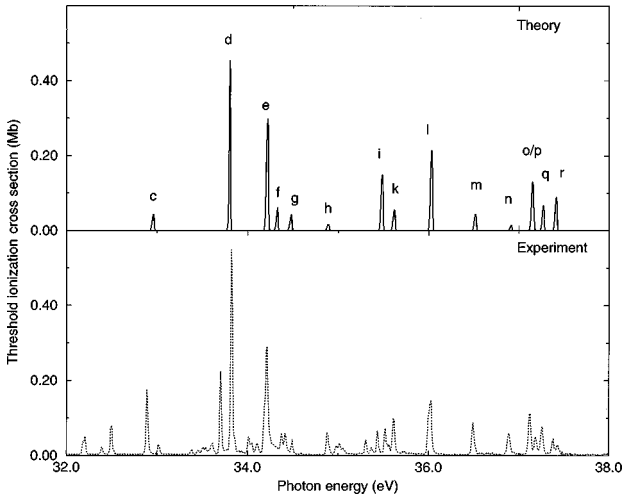

FIG. 3. Threshold photoelectron cross sections for photoionization from the Ar ground state. The present results (top) are given as a solid line, while experimental results (dotted line; bottom) are from Ref. [25]. The theoretical resonances are labeled according to the ones given in Table I. Thresholds *o* and *p* lie within 11 meV of each other, and can therefore not be separated with an experimental resolution of 25 meV.

the Rydberg series leading up to this threshold, $3p^4(^3P^e)4s\ ^2D^e$. In the present study, resonance B' lies below this threshold, but after the splitting is taken into account, this state straddles the $J=\frac{3}{2}$ level of the $3p^4(^3P^e)4s\ ^2D^e$ threshold, thereby considerably enhancing the threshold photoexcitation. The $J=\frac{1}{2}$ level of the threshold lies well above resonance B', and the threshold photoexcitation is thus not affected. This example illustrates the care required for a proper interpretation of the spectra. Another example is the $3s^23p^4(^3P^e)3d\ ^2F^e$ threshold at 34.307 eV, threshold *f*, for which the $J=\frac{9}{2}$ level is observed as a shoulder on the $3s^23p^4(^3P^e)4s\ ^2D^e$ threshold. The excitation intensity at the $3p^4(^3P^e)4p\ ^2D^o$ state at 35.5 eV, threshold *i*, agrees well with the neighboring twin peaks, but for the $3p^4(^3P^e)4p\ ^2P^o$ threshold, denoted *k*, at 35.6 eV the difference is about a factor of 2. The largest prominent discrepancy is found for the $3s^23p^4(^1D^e)3d\ ^2G^e$ state at 34.88 eV, threshold *h*, with a difference of about a factor of 3.

Between 36 and 38 eV, no quartet states of Ar^+ are found. Here the agreement between experiment and theory is poorer; for the $^2F^e$ state, threshold *l*, at 36 eV there is a 30% difference; for the $^2S^e$ state, threshold *m*, at 36.5 eV there is a factor of 2 difference; and for the $^2F^o$ state, threshold *n*, at 36.9 eV there is a difference of a factor of 3. The higher states are described much better, although the splittings into the different *J* values make this agreement less obvious. Also, autoionizing Rydberg series converging to Ar^+ states above the highest physical Ar^+ state in the calculations become important in this photon energy region. Finally, four states lie very close together between 37 and 37.3 eV, and it becomes impossible to attribute experimental peaks to individual states.

IV. CONCLUSIONS

In the present study, total photoionization and 3s photoemission cross sections for Ar are reported, focusing on the

structure observed above the threshold for $3s$ photoemission. The eigenchannel R-matrix approach has been employed using MCHF wave functions to describe the states of Ar^+ accurately using a very limited basis set. Reasonably good energies are obtained for the lowest 20 states of Ar^+ and for identifiable autoionizing states of Ar, with differences which amount to over 1.5 eV for Ar^+ states and 0.5 eV for Ar states.

In the photon energy range between 30 and 38 eV, the structure of the photoionization spectra becomes very rich due to the plethora of doubly excited states of neutral Ar. The present investigation is, to our knowledge, the first study to describe the finer details of the structure with reasonable success for both the total photoionization cross section and for the $3s$ electron emission. This agreement is obtained by including all Ar^+ states up to 38.5 eV above the Ar ground state into account. Some differences are noticeable above a photon energy of 37 eV due to the exclusion of higher Ar^+ states. Through further analysis of the photoionization spectra, the important channel interactions above the $3s3p^6$ thresholds in direct single-electron emission have been identified. The overall background cross section is described quite accurately with deviations of roughly 1.5 Mb for $3p$ emission, and 0.2 Mb for $3s$ photoemission. These differences are due to inaccuracies in the Ar ground state and the Ar^+ states, which are a consequence of the calculational strategy, which is directed to optimize the important $3p^4n\ell$ Ar^+ states.

We have also determined threshold photoionization cross sections for the lowest excited states of Ar^+, and found acceptable agreement with experiment for frequencies up to 37 eV. These calculations also take the full structure of the doubly excited states into account, within a nonrelativistic formulation and within the constraints imposed by our limited basis set size. These spectra are significantly influenced, if not dominated, by the presence of doubly excited states within 25 meV above the threshold energy. The very good agreement between theory and experiment shows that, up to a photon energy of 38 eV, the present approach is reasonably accurate. At higher frequencies, the influence of higher-lying Ar^+ states becomes important, and the expected accuracy of the calculations decreases rapidly. Nevertheless, good agreement between theory and experiment is seen up to 38 eV.

Experimental interest has also focused on the probability for leaving Ar^+ in an excited state [36–38]. Partial cross sections for photoionization with excitation of Ar^+ states have been determined for frequencies up to 42 eV [36]. As illustrated by the threshold photoionization spectra, the present calculations are able to determine these partial photoionization spectra, which will be the subject of a forthcoming paper. Recent experimental investigations have studied the fluorescence from the excited Ar^+ states created by photoionization [37,38]. The fluorescence can be measured with a much better resolution than the emitted electrons, and the resolution of the experiments is therefore significantly enhanced. Even finer details of the structure can thus be examined. Not only has the intensity of the fluorescence been investigated, but also its polarization [37,38]. These measurements provide additional information on the photoionization processes, which have received only minimal experimental and theoretical attention to date. Theoretical R-matrix results for the fluorescence polarization will also be presented in a forthcoming paper.

Other noble-gas atoms have also been investigated in experimental studies, such as the results obtained recently for Xe [39]. The present comparisons with experimental results already demonstrate the influences from spin-orbit couplings, which increase strongly with nuclear charge. For atoms heavier than Ar, jj-coupling codes will be required which incorporate the spin-orbit interaction into the Hamiltonian treated inside the R-matrix box. These more extensive calculations can presently only provide accurate results when fewer states of the ionized system are of importance. Improvements in computer technology are therefore required before present approaches can treat the photoexcitation of doubly-excited states in heavier systems to a similar extent.

ACKNOWLEDGMENTS

Discussions with F. Robicheaux are gratefully acknowledged. For this research, we used the resources of the National Energy Research Scientific Computing Center, which is supported by the Office of Energy Research of the U.S. Department of Energy under Contract No. DE-AC03-76SF00098. This work was supported by the Division of Chemical Sciences, Office of Basic Energy Sciences, Office of Energy Research, U. S. Department of Energy.

[1] R. P. Madden and K. Codling, Phys. Rev. Lett. **10**, 516 (1963).
[2] R. P. Madden, D. L. Ederer, and K. Codling, Phys. Rev. **177**, 136 (1969).
[3] J. A. R. Samson, Adv. At. Mol. Phys. **2**, 177 (1966).
[4] J. B. West and G. V. Marr, Proc. R. Soc. London, Ser. A **349**, 397 (1976).
[5] G. V. Marr and J. B. West, At. Data Nucl. Data Tables **18**, 497 (1976).
[6] O. P. Rustgi, J. Opt. Soc. Am. **54**, 464 (1964).
[7] N. Berrah, B. Langer, J. Bozek, T. W. Gorczyca, O. Hemmers, D. W. Lindle, and O. Toader, J. Phys. B **29**, 5351 (1996).
[8] J. A. R. Samson and J. L. Gardner, Phys. Rev. Lett. **33**, 671 (1974).
[9] R. G. Houlgate, J. B. West, K. Codling, and G. V. Marr, J. Electron Spectrosc. Relat. Phenom. **9**, 205 (1976).
[10] M. Y. Adam, F. Wuillemier, S. Krummacher, N. Sandner, V. Schmidt, and W. Mehlhorn, J. Electron Spectrosc. Relat. Phenom. **15**, 211 (1979).
[11] B. Möbus, B. Magel, K.-H. Schartner, B. Langer, U. Becker, M. Wildberger, and H. Schmoranzer, Phys. Rev. A **47**, 3888 (1993).
[12] O. Wilhelmi, G. Mentzel, B. Magel, K.-H. Schartner, A. Werner, S. Lauer, H. Schmoranzer, and F. Vollweiler, Phys. Lett. A **228**, 283 (1997).
[13] M. Ya. Amusia, V. K. Ivanov, and L. V. Chernysheva, Phys. Lett. A **40**, 361 (1972).

[14] E. J. McGuire, Phys. Rev. **175**, 20 (1968).
[15] A. F. Starace, Phys. Rev. A **2**, 118 (1970).
[16] M. Ya. Amusia, N. A. Cherepkov, and L. V. Chernysheva, Zh. Eksp. Teor. Fiz. **60**, 160 (1970) [Sov. Phys. JETP **33**, 90 (1971)].
[17] P. G. Burke and K. T. Taylor, J. Phys. B **8**, 2620 (1975).
[18] W. R. Johnson and K. T. Cheng, Phys. Rev. A **20**, 978 (1979).
[19] C. D. Lin, Phys. Rev. A **9**, 171 (1974).
[20] T. N. Chang, Phys. Rev. A **18**, 1448 (1978).
[21] M. P. Saha, Phys. Rev. A **39**, 2456 (1989).
[22] W. T. Silfvast, D. Y. Al-Salameh, and O. R. Wood II, Phys. Rev. A **34**, 5164 (1986).
[23] W. Wijesundera and H. P. Kelly, Phys. Rev. A **39**, 634 (1989).
[24] K. Schulz, M. Domke, R. Püttner, A. Gutiérrez, G. Kaindl, G. Miecznik, and C. H. Greene, Phys. Rev. A **54**, 3095 (1996).
[25] S. Cvejanovic, G. W. Bagley, and T. J. Reddish, J. Phys. B **27**, 5661 (1994).
[26] S. Cvejanovic and T. J. Reddish, J. Phys. B **28**, L1 (1995).
[27] M. Aymar, C. H. Greene, and E. Luc-Koenig, Rev. Mod. Phys. **68**, 1015 (1996).
[28] C. Froese Fischer, T. Brage, and A. Jönsson, *Computational Atomic Structure: An MCHF Approach* (Institute of Physics, Bristol, 1997).
[29] G. Miecznik, C. H. Greene, and F. Robicheaux, Phys. Rev. A **51**, 513 (1995).
[30] L. Minnhagen, Ark. Fys. **25**, 203 (1963).
[31] J. A. R. Samson, L. Lyn, G. N. Haddad, and G. C. Angel, J. Phys. IV C1 **1**, 99 (1991).
[32] H. Kossmann, B. Krässig, V. Schmidt, and J. E. Hansen, Phys. Rev. Lett. **58**, 1620 (1987).
[33] R. I. Hall, L. Avaldi, G. Dawber, P. M. Rutter, M. A. MacDonald, and G. C. King, J. Phys. B **22**, 3205 (1989).
[34] F. Heiser, U. Hergenhahn, J. Viefhaus, K. Wieliczek, and U. Becker, J. Electron Spectrosc. Relat. Phenom. **60**, 337 (1992).
[35] B. Krässig, J. E. Hansen, W. Persson, and V. Schmidt, J. Phys. B **29**, L449 (1996).
[36] A. A. Wills, A. A. Cafolla, F. J. Currell, J. Comer, A. Svenson, and M. A. MacDonald, J. Phys. B **22**, 3217 (1989).
[37] O. Yenen, K. W. McLaughlin, and D. Jaecks, Phys. Rev. Lett. **79**, 5222 (1997).
[38] G. Mentzel, K.-H. Schartner, O. Wilhelmi, B. Magel, U. Staude, F. Vollweier, S. Lauer, H. Liebel, H. Schmoranzer, V. L. Sukhorukov, and B. M. Lagutin, J. Phys. B **31**, 227 (1998).
[39] R. C. Shiell, M. Evans, S. Stimson, C.-W. Hsu, C. Y. Ng, J. W. Hepburn, Phys. Rev. Lett. **80**, 472 (1998).